EPJ manuscript No.
(will be inserted by the editor)

Impact of buffer gas quenching on the $^1S_0 \rightarrow ^1P_1$ ground-state atomic transition in nobelium

P. Chhetri[1,2] [a], D. Ackermann[3], H. Backe[4], M. Block[2,4,5], B. Cheal[6], Ch. E. Düllmann[2,4,5], J. Even[5,7], R. Ferrer[8], F. Giacoppo[2,5], S. Götz[2,4,5], F.P. Heßberger[2,5], O. Kaleja[2,4], J. Khuyagbaatar[2,5], P. Kunz[9], M. Laatiaoui[2,5,8], F. Lautenschläger[1,2], W. Lauth[4], E. Minaya Ramirez[10], A. K. Mistry[2,5], S. Raeder[2,5], C. Wraith[6], Th. Walther[1], and A. Yakushev[2,5]

[1] Technische Universität Darmstadt, D-64289 Darmstadt, Germany.
[2] GSI Helmholtzzentrum für Schwerionenforschung GmbH, D-64291 Darmstadt, Germany.
[3] Grand Accélérateur National d'Ions Lourds, BP 55027 - 14076 Caen Cedex 05, France
[4] Johannes Gutenberg-Universität, D-55128 Mainz, Germany.
[5] Helmholtz-Institut Mainz, D-55128 Mainz, Germany.
[6] University of Liverpool, L69 7ZE Liverpool, UK.
[7] KVI−Center for Advanced Radiation Technology, 9747 AA Groningen, The Netherlands.
[8] KU Leuven, B-3001 Leuven, Belgium.
[9] TRIUMF, Vancouver BC V6T 2A3, Canada.
[10] Institut de Physique Nucléaire Orsay, 91406 Orsay, France.

Received: date / Revised version: date

Abstract. Using the sensitive Radiation Detected Resonance Ionization Spectroscopy (RADRIS) technique an optical transition in neutral nobelium (No, Z=102) was identified. A remnant signal when delaying the ionizing laser indicated the influence of a strong buffer gas induced de-excitation of the optically populated level. A subsequent investigation of the chemical homologue, ytterbium (Yb, Z=70), enabled a detailed study of the atomic levels involved in this process, leading to the development of a rate equation model. This paves the way for characterizing resonance ionization spectroscopy (RIS) schemes used in the study of nobelium and beyond, where atomic properties are currently unknown.

PACS. 3 2.80.-t, 32.70.Cs, 33.50.Hv

1 Introduction

Atomic structure studies of elements beyond fermium (Fm, Z=100) are one of the most interesting and challenging disciplines of atomic physics [1]. A major question concerns the influence of strong relativistic effects on the valence electron configuration of the atom, and its consequence on the level structure and the chemical behaviour. For almost a decade, fermium was the heaviest element for which a direct identification of atomic levels was performed. This was achieved using laser spectroscopy in a buffer-gas cell in combination with ion detection [2]. Elements with Z>100 (transfermium elements) are produced in accelerator-based nuclear fusion-evaporation reactions at very low rates. Therefore, spectroscopic investigations could only recently be accomplished successfully when the $^1S_0 \rightarrow ^1P_1$ ground state transition in nobelium was observed [3]. A novel ultra-sensitive experimental method was applied, based on the Radiation Detected Resonance Ionization Spectroscopy (RADRIS) [4]. A successful two-step resonance-ionization process with pulsed lasers, in a buffer gas cell is detected via the characteristic α−decay of the investigated nuclei [5,6,7]. To this end, the first excitation step resonantly excites an atomic state while the second step non-resonantly ionizes the atom. The lifetime of the excited atomic state can be determined by delaying the second laser pulse relative to the first. In the presence of argon buffer gas, a signal was still observed when the second, ionizing step from the intermediate $^1P_1$ state to the continuum was delayed with respect to the first step [3]. Although the lifetime for the $^1P_1$ state was calculated to be in the range between 2.0 and 3.7 ns [8,9,10], the observed tail indicated lifetimes of the order of 100 ns or even longer. Hence, it is conjectured that the $^1P_1$ state population undergoes a fast quenching transition into at least one metastable state from which resonance ionization may occur as well. Buffer gas induced population transfer in resonant ionization has also been reported in [11], where a three-step ionization scheme developed for vacuum application did not work in a buffer gas environment. These facts prompted us to investigate the effect of gas-induced quenching of atomic states in the chemical homologue, Yb, a stable element with a similar atomic level structure as

[a] email:P.chhetri@gsi.de

No. A derived rate equation model described all observations and enabled the extraction of relevant parameters for the optical transition of interest. This was verified for Yb and finally applied to the No data, resulting in a congruent description of the complete data set composed of a long decay in delayed ionization spectra, a fast saturation of the transition as well as a strong saturation broadening in the resonance spectra.

In this article the structure of an effective level scheme and the corresponding rate equation model are discussed, guided by resonance ionization results with a natural isotope composition of Yb (^{nat}Yb). Complementing these measurements with reported literature values on atomic levels, transition strengths and atomic lifetimes [12,13,14,15,16], a qualitative and quantitative explanation of the quenching mechanism is demonstrated. Finally, the rate equation model is applied to the results obtained from the laser spectroscopy on No and the strength of the observed transition is deduced. Furthermore, the impact of quenching on the search for Rydberg states in No is discussed.

2 Experimental setup

A detailed description of the on-line RADRIS set-up can be found in [3,4,5,6,7]. The off-line measurements on ^{nat}Yb were performed in a dedicated off-line set-up schematically shown in Fig. 1. In this off-line cell, a 25 μm thick foil of metallic Yb was clamped onto a 12.5 μm thick tantalum foil. It was resistively heated to evaporate Yb atoms. A two step photo-ionization was applied, using tunable dye lasers pumped by excimer lasers whereby the non-resonant second step was provided by an excimer laser at wavelength 351 nm such that the total energy of the broadband radiation from both steps was higher than the ionization potential of 6.254159 eV [17]. The laser systems were operated at a repetition rate of 100 Hz, which is well suited for these measurements as discussed in more detail in [7,18]. The dye laser radiation was transported to the experimental set-up by UV fibres and finally collimated into the buffer gas cell filled with argon by an output coupler with a 2 inch lens of 75 mm focal length. The excimer lasers were individually triggered and feature an intrinsic jitter with respect to the trigger pulse of typically 8 ns at a laser pulse duration of about 18 ns. The individual triggering in combination with a high-precision multichannel pulser (BNC Model 550) enabled measurements of delayed ionization, mapping the lifetime of excited states. The created photo-ions were transported by electric fields to a wire connected to a charge-sensitive preamplifier, where the accumulated charge, was detected in coincidence with the laser pulse. The signal amplitude, which is proportional to the number of produced photo-ions, was recorded in conjunction with the set wavenumber and the delay time.

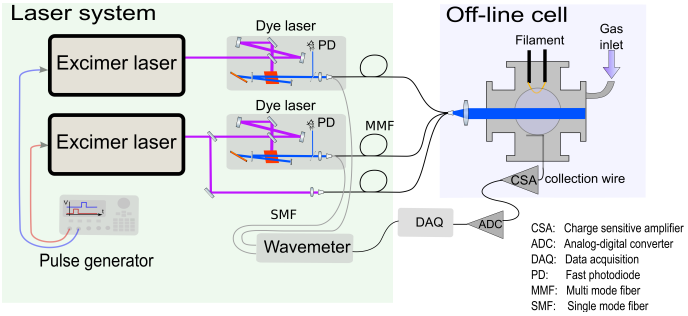

Fig. 1. Schematic overview of the off-line measurement set-up comprising of the off-line buffer gas cell along with the laser and the DAQ system.

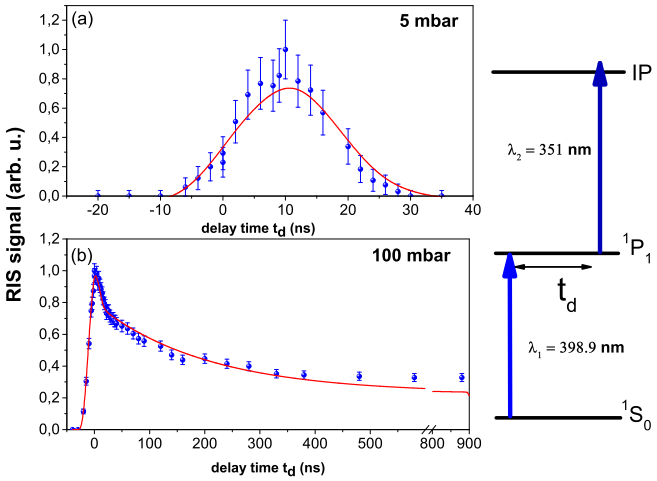

Fig. 2. Ion signal for two-step excitation scheme with non-resonant second step as shown in the right panel for different laser pulse delays in ^{nat}Yb at 5 mbar (a) and at 100 mbar (b) argon gas pressures. The solid line represents the best fit of the data using the 5-level rate equation model, see Section 3.

3 Rate equation model

The off-line resonance ionization spectroscopy of ^{nat}Yb at 100 mbar argon pressures, revealed a remnant signal for delayed ionization processes similar to the observation in on-line experiments on No, see Fig. 2. Here, the resonance ionization signal strength is shown as a function of different delay times (t_d) between the two laser pulses exciting the first and second step. The first, resonant step was tuned to excite the $^1P_1$ level from the $^1S_0$ ground state at a vacuum wavelength of 398.9 nm. The second laser provided light at 351 nm for non-resonant photoionization. At a gas pressure of 5 mbar (Fig. 2 (a)), the observed fast decrease in the RIS signal is in agreement with the lifetime of 5 ns reported in [14,15,16] for the populated $^1P_1$ level. Note that the rising and the falling edge as well as the decay behaviour is also influenced by the temporal shape of the laser pulses. When increasing the argon pressure to about 100 mbar (Fig. 2 (b)) the RIS signal slowly decreases in the course of time and cannot be described, *e.g.* by a single exponential. This implies that a simple 2-level system does not fully describe the considered ionization

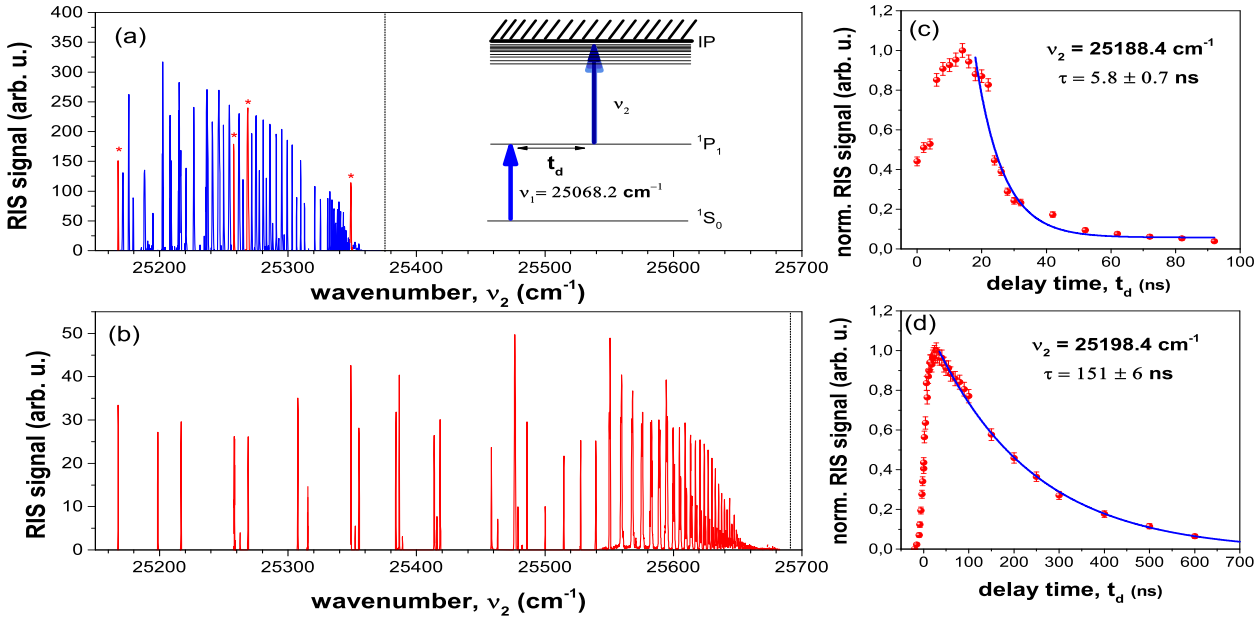

Fig. 3. Rydberg states in ^{nat}Yb (a) for prompt ionization with $t_d = 0$ ns and (b) for delayed ionization with $t_d = 60$ ns with the dashed lines indicating their convergence (series limit) from the Rydberg-Ritz fit. States marked with * in (a) represent Rydberg states of counterparts (b) which proceeded via an intermediate state. (c) RIS signal for delayed Rydberg excitation proceeding via the $^1P_1$ intermediate state. The decay time constant extracted from an exponential fit to the data (solid line) matches with the lifetime reported in the literature for the $^1P_1$ level. (d) Same as in (c) for ν_2= 25198.4 cm^{-1}. In this case, an extended decay time is extracted, which is attributed to the lifetime of the intermediate state, the $^3D_2$ level at 24751.948 cm^{-1} via which the excitation into the Rydberg states is proceeding. All the measurements were performed at a gas pressure of about 100 mbar. See text for more information.

process and that the implementation of a multi-level system is necessary to accurately determine the parameters of the optical transition.

The quenching of atomic levels in a gas environment is reported in similar systems, *e.g.* in atomic barium [19] and calcium [20]. From the laser pulse duration of about 18 ns in our experiment, a lower limit on the de-excitation rate can be estimated to be of the order of 10^8 s^{-1}, which is much larger than values in noble gases for energy gaps of the order of 1000 cm^{-1}. As the quenching rate is in general inversely proportional to the energy gap, as discussed for fine-structure levels in [21], this indicates the influence of states that are closer in energy, such as the $^3D_2$ level in Yb, which is 316 cm^{-1} below the $^1P_1$ level [12,13].

To determine the levels involved in the quenching process, we performed off-line measurements on Rydberg levels, excited from intermediate excited states in ^{nat}Yb. For this purpose, a dye laser was operated at a vacuum wavelength of 398.9 nm exciting the $^1P_1$ state. A second tunable dye laser was then used to scan Rydberg states. Figure 3 (a) shows the obtained spectrum when both laser pulses arrive at the cell simultaneously. Members of at least two Rydberg series were observed. The most prominent series agrees with reported Rydberg states belonging to s- and d-series [22], which can be directly excited from the $^1P_1$ level, populated by the first step. This first series vanishes when delaying the second laser pulse, *e.g.* by 60 ns, leaving a Rydberg series proceeding via an intermediate state visible in the spectrum (Fig. 3 (b)). Comparing the convergence of the two series, indicated by the dashed lines in Fig. 3 (a) and (b), which differ by 316 cm^{-1} it becomes obvious that the latter Rydberg series have proceeded via the $^3D_2$ level. The population of the $^3D_2$ state by gas-induced quenching was verified by analyzing the gas pressure dependence of the relative RIS-signal strengths when ionizing via Rydberg levels excited either from the $^1P_1$ or the $^3D_2$ state. Further Rydberg states attributed to other series excited from the lower lying $^3D_1$ state (579 cm^{-1} below the $^1P_1$ state), were also seen, but are at least a factor of 100 times lower in intensity and can therefore be neglected in the construction of the effective level scheme for the rate equation model.

Additional investigations concentrated on measurements with a delayed second excitation step (via Rydberg states), probing the lifetime of the intermediate states. Figure 3 (c) and (d) shows the observed lifetimes of the $^1P_1$ and the $^3D_2$ state, respectively. Even at a gas pressure of about 100 mbar, the short lifetime of the $^1P_1$ level can be deduced from this measurement, as shown in Fig 3 (c). However, for the $^3D_2$ level, see Fig 3 (d), the deduced lifetime of 154 ns is significantly shorter than the reported value of 460 ns [14,15,16], indicating that a subsequent quenching to energetically lower states may be present and thus contributing to the loss of the RIS signal, Fig. 3 (d).

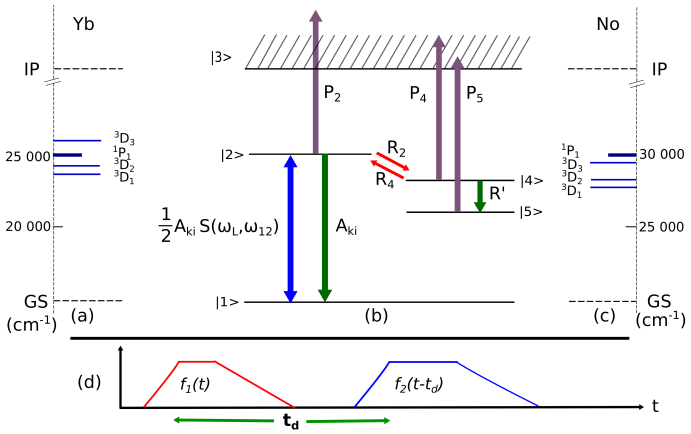

Fig. 4. (a) Atomic structure of Yb [12,13,14,15,16]. (b) A level scheme with radiative and non-radiative processes used in the rate equation model developed to describe the experimental data. (c) Predicted atomic structure of No [8,9,10]. (d) Laser pulse shape assumed for the exciting and ionizing step.

Therefore, in an effective level scheme, only one close-lying additional level in which the $^1P_1$ population is transferred by gas collision induced quenching was implemented, see Fig. 4. Nevertheless, the results from the delayed non-resonant ionization in Fig. 2(b) show that there is also a very long-lived state contributing to the RIS signal, besides the short-lived $^1P_1$ ($|2\rangle$) and the longer-lived $^3D_2$ ($|4\rangle$) states. Atomic states featuring long lifetimes, such as the $^3P_2$ level or the $4f^{13}5d_{3/2}6s^2$ $J = 2-5$ ($|5\rangle$) levels in Yb may serve for collecting the population from gas collisional de-excitation of higher lying levels. Thus, an effective 5-level-scheme (ground state ($|1\rangle$), three intermediate states and an ionic state ($|3\rangle$)), Fig. 4(b), is suitable to describe the experimental observations. Considering the broadband laser pulse in our experiment, the coherence terms in the optical Bloch equation can be neglected [23], and an effective rate equation model can be formulated:

$$\frac{d\rho_1}{dt} + \frac{1}{2}(\rho_1 - \rho_2)A_{ki}S(\omega_L,\omega_{12})f_1(t) = A_{ki}\rho_2$$
$$\frac{d\rho_2}{dt} + \big[A_{ki} + R_2 + P_2 f_2(t-t_d)\big]\rho_2 = \frac{1}{2}(\rho_1 - \rho_2)A_{ki}S(\omega_L,\omega_{12})f_1(t) + R_4\rho_4$$
$$\frac{d\rho_3}{dt} = (P_2\rho_2 + P_4\rho_4 + P_5\rho_5)f_2(t-t_d)$$
$$\frac{d\rho_4}{dt} + \big[R' + R_4 + P_4 f_2(t-t_d)\big]\rho_4 = R_2\rho_2$$
$$\frac{d\rho_5}{dt} + P_5 f_2(t-t_d)\rho_5 = R'\rho_4$$

with the normalization

$$\sum_i \rho_i = 1$$

and the initial conditions

$$\rho_1(t=0) = 1 \text{ and } \rho_i(t=0) = 0 \text{ for } 1 < i$$

where ρ_i, with $i = 1-5$, corresponds to the occupation of individual states $|i\rangle$, A_{ki} is the Einstein coefficient for spontaneous emission for the $^1P_1 \rightarrow {}^1S_0$ transition, which is related to the radiative lifetime τ_{ki} of the excited state by $A_{ki} = \tau_{ki}{}^{-1}$. $R_{2,4}$ are the quenching rates from the $^1P_1$ state to the lower-lying intermediate state (e.g. $^3D_2$ ($^3D_3$) in the case of Yb (No)) and back to the $^1P_1$ state, respectively. R' is the effective transfer rate to the long-lived state, where the population transfer is composed of optical decay as well as non-radiative decays due to gas collisions. $f_1(t)$ and $f_2(t-t_d)$ refer to the laser pulse shapes for the first- and second-excitation steps, respectively, as shown in Fig. 4(d). t_d is the time delay of the ionizing laser with respect to the first-excitation step. The ionizing rates P_j are defined as

$$P_j = \frac{E_2/A_2}{t_2\hbar\omega_2}\sigma_j \quad \text{, with } j = 2,4,5$$

where E_2/A_2 is the second-step laser pulse energy per unit area, t_2 the laser pulse duration, $\hbar$ is the reduced Planck constant, ω_2 the angular frequency of the ionizing laser and σ_j the ionization cross-section. The frequency-dependent saturation parameter $S(\omega_L,\omega_{12})$ is given by

$$S(\omega_L,\omega_{12}) = \frac{\lambda_1^2}{2}\frac{E_1/A_1}{t_1\hbar\omega_{12}}\int \frac{1}{\sqrt{2\pi}\sigma_\omega} exp\Big[-\frac{(\omega-\omega_L)^2}{2\sigma_\omega^2}\Big] \frac{\gamma_\omega'/2\pi}{(\omega-\omega_{12})^2 + (\gamma_\omega')^2/4}d\omega,$$

where E_1/A_1 is the first-step laser pulse energy per unit area, λ_1 is the corresponding wavelength, t_1 is the laser pulse duration and ω_{12} is the resonance frequency of the first step. The spectral distribution is described as a convolution of a Gaussian function with a Lorentzian profile. The spectral laser profile (σ_L) and the Doppler broadening (σ_D) contribute to the Gaussian part according to $\sigma_\omega^2 = \sigma_L^2 + \sigma_D^2$ centred around the laser frequency ω_L. The natural line width of the transition, the collisional dephasing (τ_{coll}) and dephasing due to the phase fluctuations of different laser modes (τ_{mode}) contribute to the Lorentzian part of the width γ_ω' according to

$$\gamma_\omega' = \frac{1}{2\pi}\Big(A_{ki} + \frac{1}{\tau_{coll}} + \frac{1}{\tau_{mode}}\Big).$$

The rate equations were solved by integrating over the time t and adapted to the data obtained for the first-step resonance, for the saturation curve and for the delayed RIS signal. This model was fitted to the resonance spectra and to the saturation of the ground state optical transitions in Yb and No using a χ^2 minimization algorithm, implemented in the minuit package of the root evaluation software [24].

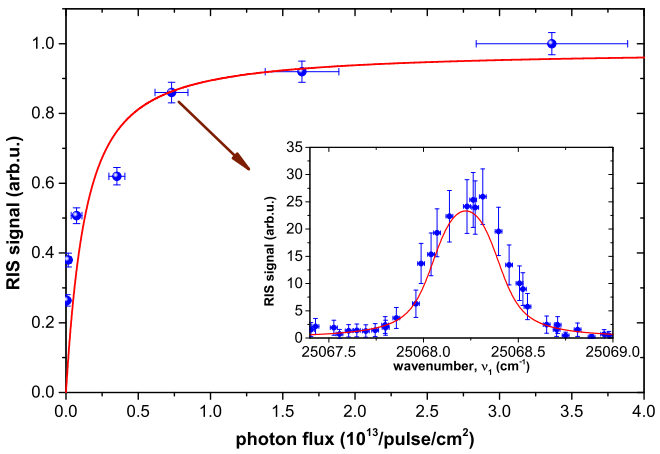

Fig. 5. The saturation curve of the $^1S_0 \rightarrow ^1P_1$ transition in ^{nat}Yb. The signal at resonance normalized to the maximum. The photon flux for the ionizing laser was 4.1×10^{14} photons/pulse/cm^2. Inset: Wavenumber scan around the first-step resonance at 25068.22 cm^{-1} in ^{nat}Yb. The arrow indicates the photon flux of the first laser step at which the resonance (inset) was measured. The solid line represents the best fit using the 5-level rate equation model to the data.

4 Measurements and results

4.1 Off-line measurements on stable Yb

To check the validity of the formulated model, extensive off-line measurements were performed on ^{nat}Yb for which the atomic level scheme is well known [12,13,14,15,16]. For resonance ionization spectroscopy, the dye laser was tuned to excite the $6s6p\ ^1P_1$ state located at 25068.22 cm^{-1}. The excited atoms were non-resonantly ionized by high-power laser radiation from the excimer laser operated at 351 nm. Figure 5 shows the saturation characteristics of the $^1S_0 \rightarrow ^1P_1$ transition when changing the pulse energy of the first-excitation step. The inset shows the spectral profile of the resonance at a photon flux of 7×10^{12} photons/pulse/cm^2. The measurements were carried out at an argon gas pressure of about 100 mbar. The solid lines represent the best fit from the rate equation model. Here the fit was performed for the transition strength expressed by the Einstein coefficient A_{ki}, while the other parameters have been fixed to the values summarized in Tab. 1. These values have been validated by fitting the rate equation model to the data from the measurements with a delayed ionization scheme shown in Fig. 2(a) and (b), where the solid line corresponds to the best fit obtained. The Doppler broadening contribution, here denoted by (σ_D), is deduced from the gas temperature which is assumed to be at $T = 300$ K and the measured laser bandwidth with $\sigma_L = 2.5$ GHz. The time scale of collisional dephasing (τ_{coll}) can be calculated from the collision rate in 100 mbar argon gas by $\tau_{coll}^{-1} \approx \sigma_{coll} N \sqrt{\frac{8kT}{\pi \mu_{Ar,No}}}$, where σ_{coll} is taken as 1×10^{-13} cm^2 [25], N is the density of the gas at 100 mbar and $\mu_{Ar,No}$ is the reduced mass. The time scale of the mode fluctuations in the laser pulse (τ_{mode}) is taken similar as in [26]. The quenching rate from the $^1P_1$ level to the closest $^3D_2$ energy level (R_2) is 8×10^7 s^{-1} and therefore half of the value of the optical decay rate to the ground state. The back pumping rate (R_4) can be assumed to be negligibly small, as expected from detailed balance considerations. The combined quenching and optical decay rate of the $^3D_2$ level (R') is more than one order of magnitude weaker in comparison to R_2, which is also reflected in the sustainable RIS signal observed in the delayed ionization via Rydberg levels, Fig. 3. The ionization rates from the $^1P_1$ and the $^3D_2$ (P_2 and P_4) state are identical as can be expected from the non-resonant character of the ionization process and the fact that both excited levels were energetically close to each other. Nevertheless, the ionization rate (P_5) from the longest-lived state is assumed to be one order of magnitude smaller. A small deviation at a relatively long delay time as seen in Fig. 2 (b) points to the influence of additional energetically lower-lying levels. However, the consideration of an addition level did not have any significant impact on the fit results. Thus, in order to reduce the number of free parameters a 5-level system was chosen. The obtained Einstein coefficient $A_{ki} = 2.5 \pm 0.6 \times 10^8$ s^{-1} is in agreement with the literature value of $A_{ki}^{\ lit} = 1.9 \times 10^8$ s^{-1} [14].

Table 1. Parameters taken as constants, that were used to fit the data

Parameter	No	Yb	Unit
σ_ω	2.5	2.5	GHz
$\tau_{coll}^{\ -1}$	11	11	GHz
$\tau_{mode}^{\ -1}$	9	9	GHz
R'	0.01×10^9	0.006×10^9	s^{-1}
P_2	0.05×10^9	0.05×10^9	s^{-1}
P_4	0.05×10^9	0.05×10^9	s^{-1}
P_5	0.003×10^9	0.003×10^9	s^{-1}
R_2	0.3×10^9	0.08×10^9	s^{-1}
R_4	0	0	s^{-1}

4.2 On-line measurements on ^{254}No

After having established and validated the model based on RIS measurements on Yb, it was applied to the radioactive nobelium data reported in [3]. The isotope ^{254}No ($T_{1/2} = 51.2$ s) was produced in the fusion-evaporation reaction ^{208}Pb(^{48}Ca, 2n)^{254}No with a cross section of 2 μb at a primary beam energy of 4.55 A·MeV [27]. For these measurements the RADRIS set-up was operated behind the velocity filter SHIP at GSI, Darmstadt. The filter is used to separate the nuclear reaction products from the accelerated ^{48}Ca beam [28].The nobelium atoms were stopped in a buffer-gas cell filled with 95 mbar argon and were subsequently guided onto a thin tantalum filament. After a suitable collection time the primary beam was blocked and the accumulated ions were re-evaporated from the filament as neutral atoms by heating it to a temperature of 1050 K for 0.3 s. A two-step photoionization process was

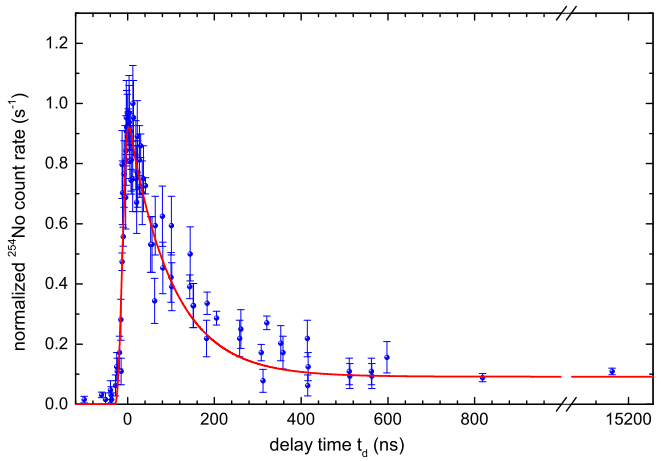

Fig. 6. Normalized $\alpha-$decay rate as a function of the delay time t_d between the first- and the second-step excitations in ^{254}No. The solid line indicates the best fit to the data from the rate equation model.

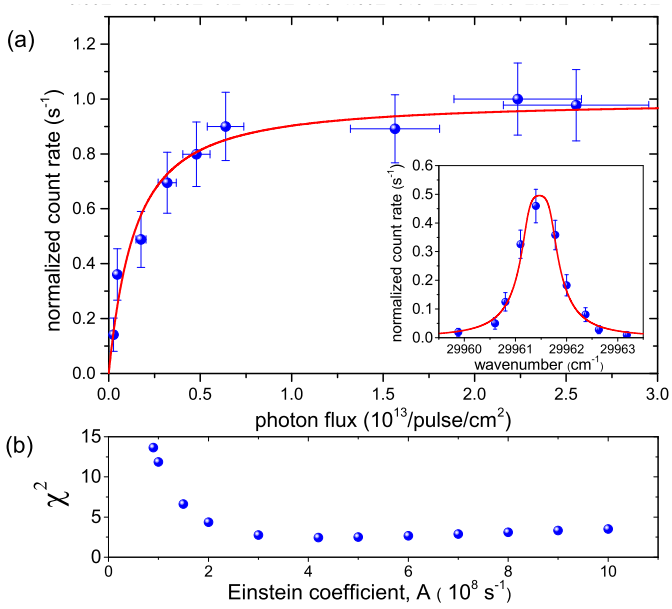

Fig. 7. (a) Saturation of the $^1S_0 \rightarrow ^1P_1$ transition in ^{254}No with the best fit to the data (red curve). Inset: Spectral profile of the ^{254}No resonance. The solid curve represents the best fit to the data from the rate equation model resulting in a full width at half-maximum (FWHM) of 0.80 cm^{-1}. (b) χ^2 values obtained when applying the model with different A_{ki}.

applied to ionize the atoms. Photo-ions were then transported onto a silicon detector and were identified by their characteristic $\alpha-$decay energy.

The involvement of additional intermediate atomic states in the ionization process in No in analogy with Yb was clear when measuring the RIS signal for a delayed non-resonant, second laser pulse as shown in Fig. 6. The ^{254}No alpha decay rate was recorded as a function of the ionizing laser delay time (t_d), while keeping the laser power of both excitation steps constant. A RIS signal component that exponentially decreases with a lifetime on the order of 100 ns was visible, as well as a contribution from levels with much longer lifetimes. From the predicted level scheme for No (Fig. 4) the $^3D_3$ state is expected to be energetically much closer to the $^1P_1$ state [8,29], in comparison to the $^3D_2$ state in the case of Yb, which will nevertheless not alter the effective level scheme presented in Fig. 4. Applying the rate equation model to the data (solid line), allows validation of the parameter set summarized in Tab. 1. The result was then used for the investigation of the first-step saturation behaviour. In comparison to Yb, the quenching rate (R_2) of the $^1P_1$ state is larger, which is directly obvious from the absence of a short-lived component in the signal for the delayed ionization, Fig. 6.

During the saturation measurement (Fig. 7 (a)) the first excitation step was kept at resonance and the $\alpha-$decay rate was measured as a function of the laser power of this excitation step. The photon flux of the ionizing step was kept as high as 7.3×10^{15} photons/pulse/cm^2 leading to the saturation of the ionization process. The rate equation model was fitted to the data for different values of the Einstein coefficient A_{ki} and the resulting χ^2 values are shown in Fig. 7(b) featuring an asymmetric confidence band. As the power measurements and the laser spot size determination are prone to systematic uncertainties, the data was also evaluated for a conservative estimate of a 20% increased and a 20% decreased photon flux respectively, to account for the systematic uncertainty in the determination of the photon flux. Different laser pulse shapes, from a rectangular to a trapezoidal shape with a pulse duration of 18 ns, were also considered leading to an Einstein coefficient of $A_{ki} = 4.2^{+2.6}_{-2.8}\times10^8$ s^{-1} for the first-step transition. Though the uncertainty from the fit seems to be large, a weak transition with an Einstein coefficient below 1×10^8 s^{-1} can be ruled out from the χ^2 analysis (Fig. 7 (b)). Figure 7(a) (inset) shows the observed resonance in ^{254}No when varying the excitation frequency of the first excitation step at a fixed photon flux of 1.1×10^{14} photons/pulse/cm^2. The best fit is shown as a solid line and results in a resonance centre of 29961.46 $\pm$0.01 cm^{-1} [3].

5 Summary

Resonance ionization spectroscopy of No was performed in a buffer gas using the RADRIS technique. An observed collisional de-excitation of the optically excited state to lower-lying states, was confirmed in similar off-line measurements using ^{nat}Yb. These studies performed on the homologue led to the development of an effective 5-level rate equation model sufficient to describe the observations for both elements. In combination with delayed ionization measurements this gives access to the lifetimes to the $^1S_0 \rightarrow ^1P_1$ ground state transition and excitation energies of further states in nobelium, and their unambiguous identification.

Rydberg states could be identified from the direct excitation from the short-lived $^1P_1$ state in Yb, even at pres-

sures around 100 mbar. However, for non-resonant ionization the population transfer to longer lived states offered an enhancement of the RIS efficiency, reducing the sensitivity to the temporal jitter of the laser pulses. For schemes where this second step was resonant, it was possible to compare the limits of convergence of the Rydberg series and so determine the relative energies of the intermediate levels. This would otherwise have been impractical due to transitions from the ground state being forbidden. These studies will be invaluable in developing future RIS schemes and reliably interpreting the processes involved. Similar investigations will be crucial in extracting the atomic properties of the heaviest elements.

Acknowledgements

This work was supported by the German Federal Ministry of Research under contracts 06MZ169I, 06LM236I, FAIR NuSTAR 05P09RDFN4, 05P12RDFN8, and 05P15RDFN1. This project has also received funding from the European Unions Horizon 2020 research and innovation programme under grant agreement no. 654002 (ENSAR2)

References

1. H. Backe *et al.*, Nucl. Phys. A **944**, 492 (2015)
2. M. Sewtz *et al.*, Phys. Rev. Lett. **90**, 163002 (2003)
3. M. Laatiaoui *et al.*, Nature **538**, 495 (2016)
4. H. Backe *et al.*, Hyperfine Interact. **78**, 35 (1993)
5. H. Backe *et al.*, Eur. Phys. J. D **45**, 99 (2007).
6. M. Laatiaoui *et al.*, Eur. Phys. J. D **68**, 71 (2014)
7. F. Lautenschläger *et al.*, Nucl. Instrum. Methods B **383**, 115 (2016)
8. A. Borschevsky *et al.*, Phys. Rev. A **75**, 042514 (2007)
9. Y. Liu *et al.*, Phys. Rev. A **76**, 062503 (2007)
10. P. Indelicato *et al.*, Eur. Phys. J. D **45**, 155 (2007)
11. I. Pohjalainen et al. Nucl. Instrum. Methods B **376**, 233 (2016)
12. Kramida, A., Ralchenko, Yu., Reader, J., and NIST ASD Team (2015). NIST Atomic Spectra Database (ver. 5.3). Available: http://physics.nist.gov/asd [2016, May 31].
13. W. Meggers and J. Tech, J. Res. Nat. Bureau Stand. **83**, 13 (1978)
14. K. B. Blagoev *et al.*, At. Data Nucl. Data Tables **56**, 33 (1994)
15. C. J. Bowers *et al.*, Phys. Rev. A **5**, 533103 (1996)
16. S. G. Porsev *et al.*, Phys. Rev. A **4**, 602781 (1999)
17. M. Aymar *et al.*, J. Phys B **13**, 1089 (1980)
18. M. Laatiaoui *et al.*, Hyperfine Interact. **227**, 69 (2014)
19. J. Brust and A. C. Gallagher, Phys. Rev. A **52**, 2120 (1995)
20. W. H. Pence and S. R. Leone, J. Chem. Phys. **74**, 5707 (1981)
21. L. Krause, Phys. El. Atomic Coll.l., VlII ICPEAC (Amsterdam: North Holland), 65 (1972)
22. P. Camus *et al.*, J. Phys. B: Atom. Molec. Phys. **13**, 1073 (1980)
23. R. Loudon, *The Quantum Theory of Light* (OUP Oxford, 2000.)
24. F. James, MINUIT Function Minimization and Error Analysis, Reference Manual Version 94.1, CERN Program Library Long Writeup D506,
25. A. Corney, *Atomic and laser spectroscopy* (Oxford: Clarendon Press, 1978)
26. M. Sewtz, Ph.D. thesis, Johannes Gutenberg-Universität, Mainz, 2003
27. M. Leino *et al.*, Eur. Phys. J. A **6**, 63 (1999)
28. G. Münzenberg *et al.*, Nucl. Instrum. Meth. **161**, 65 (1979)
29. V.A. Dzuba *et al.*, Phys. Rev. A **90**, 012504 (2014)